Journal of Clinical Monitoring and Computing (2021) 35:1325–1332
https://doi.org/10.1007/s10877-020-00598-5

ORIGINAL RESEARCH

A mathematical model for predicting intracranial pressure based on noninvasively acquired PC-MRI parameters in communicating hydrocephalus

Jia Long[1,2] · Deshun Sun[3] · Xi Zhou[2] · Xianjian Huang[4] · Jiani Hu[5] · Jun Xia[2] · Guang Yang[6,7]

Received: 10 June 2020 / Accepted: 22 September 2020 / Published online: 1 October 2020
© Springer Nature B.V. 2020

Abstract

To develop and validate a mathematical model for predicting intracranial pressure (ICP) noninvasively using phase-contrast cine MRI (PC-MRI). We performed a retrospective analysis of PC-MRI from patients with communicating hydrocephalus (n = 138). The patients were recruited from Shenzhen Second People's Hospital between November 2017 and April 2020, and randomly allocated into training (n = 97) and independent validation (n = 41) groups. All participants underwent lumbar puncture and PC-MRI in order to evaluate ICP and cerebrospinal fluid (CSF) parameters (i.e., aqueduct diameter and flow velocity), respectively. A novel ICP-predicting model was then developed based on the nonlinear relationships between the CSF parameters, using the Levenberg–Marquardt and general global optimisation methods. There was no significant difference in baseline demographic characteristics between the training and independent validation groups. The accuracy of the model for predicting ICP was 0.899 in the training cohort (n = 97) and 0.861 in the independent validation cohort (n = 41). We obtained an ICP-predicting model that showed excellent performance in the noninvasive diagnosis of clinically significant communicating hydrocephalus.

Keywords Intracranial pressure · Phase-contrast cine MRI · Cerebrospinal fluid parameters · Communicating hydrocephalus · Levenberg–marquardt optimisation

Jia Long and Deshun Sun have contributed equally to this work.

✉ Jun Xia
xiajun@email.szu.edu.cn

Jia Long
halo771@163.com

Deshun Sun
13240766843@163.com

Xi Zhou
xizhoudoctor@163.com

Xianjian Huang
ken_1978@163.com

Jiani Hu
jhu@med.wayne.edu

Guang Yang
g.yang@imperial.ac.uk

[1] Department of Radiology, Pinghu Hospital Shenzhen University, Shenzhen, China

[2] Department of Radiology, Shenzhen Second People's Hospital, Health Science Center, The First Affiliated Hospital of Shenzhen University, Shenzhen, China

[3] Shenzhen Key Laboratory of Tissue Engineering, Shenzhen Laboratory of Digital Orthopedic Engineering, Guangdong Provincial Research Center for Artificial Intelligence and Digital Orthopedic Technology, Shenzhen Second People's Hospital, Health Science Center, The First Hospital Affiliated To Shenzhen University, Shenzhen 518035, China

[4] Department of Neurosurgery, Shenzhen Second People's Hospital, Health Science Center, The First Affiliated Hospital of Shenzhen University, Shenzhen 518035, China

[5] Department of Radiology, School of Medicine, Wayne State University, Detroit, MI 48201, USA

[6] Cardiovascular Research Centre, Royal Brompton Hospital, London SW3 6NP, UK

[7] National Heart and Lung Institute, Imperial College London, London SW7 2AZ, UK

1 Introduction

Invasive monitoring via lumbar puncture is the current reference standard for measuring intracranial pressure (ICP) for the diagnosis and management of chronic disorders, including hydrocephalus [1]. Several clinical practice guidelines state that invasive ICP monitoring can also be considered in other patient groups where there are concerns about elevated pressure and/or impaired cerebral perfusion [2–4]. However, invasive ICP monitoring is not suitable in all settings, e.g., when immediate treatment for elevated ICP is required, particularly emergency departments, rural areas, and resource-poor settings [5]. Moreover, at most centres, only neurosurgeons are trained to use this invasive procedure [6], which requires the insertion of an ICP monitor that may result in several vital complications, including haemorrhage and infection [7, 8].

Noninvasive methods that have consequently been explored to estimate the ICP include the use of ultrasound signals to measure cerebral blood flow velocity indices [9], brain tissue resonance [10], skull vibrations [11], transcranial time of flight [12], optic nerve sheath diameter assessment [13], venous ophthalmodynamometry [14], otoacoustic emissions analysis [15], tympanic membrane displacement sensing [16], incremental intracranial compliance (and thereby ICP) estimations based on magnetic resonance imaging [17, 18], and visual evoked potential recordings [19]. However, all of these techniques have their limitations and have potentially low clinical utility. For example, transcranial Doppler sonography could not be used for 10–15% of the patients due to the ultrasound not being able to penetrate the skull [20]. Because of the perilymphatic duct being less passable with age, tympanic membrane displacement measurements have relatively low practicability [21]. Moreover, venous ophthalmodynamometry could be applied only in patients with elevated ICP without papilledema [21].

Phase-contrast cine MRI (PC-MRI) can be used to acquire information on fluid dynamics noninvasively with computer-aided modelling. In our previous study [22], we have identified nonlinear relationships between ICP and two PC-MRI-derived quantitative CSF parameters, i.e., aqueduct diameter and flow velocity. We have found that the ICP is increased with an average velocity above 1.628 cm/s ($P < 0.001$), and aqueduct diameter more than 3.6 mm ($P \leq 0.01$). In this study, we aimed to further develop a novel mathematical model that can be used to evaluate these noninvasively acquired ICP-associated parameters based on their correlations. We demonstrate the accuracy of our ICP-predicting model for potential clinical use in the diagnosis and management of communicating hydrocephalus.

2 Materials and methods

2.1 Patients and management

This study included 138 participants recruited from Shenzhen Second People's Hospital between November 2017 and April 2020, retrospectively. All the included patients were diagnosed with communicating hydrocephalus and underwent lumbar puncture and PC-MRI examinations on the same day. These participants were randomly divided into training ($n = 97$) and independent validation ($n = 41$) groups for our model development and verification. Age, sex, heart rate, blood pressure, and body weight and height (used to calculate body mass index, BMI) were recorded for all the participants. The data collection methods were the same as those described in our previous study [22]. This study was approved by the local hospital Human Research Ethics Committee and was in accordance with the relevant provisions of the Helsinki Declaration on the ethics of clinical research. Informed consent was obtained from all the patients.

Inclusion criteria: (I) patients with clinical suspected or diagnosed communication hydrocephalus. (II) MRI showing ventricular enlargement, Evan's index was greater than 0.3, but with normal sulcus. Exclusion criteria: (I) patients with complete obstructive hydrocephalus. (II) patients unsuited or unwilling to do a lumbar puncture and MRI. (III) suboptimal image quality for assessment and clinical diagnosis.

2.2 Magnetic resonance imaging sequences

All MRI images were obtained using a 3.0 T MRI scanner (Prisma, Siemens, Erlangen, Germany) with 20-channel phase-array head coils. All patients underwent conventional MRI scanning, including axial T2WI and a retrospective cardiac-gated phase contrast flow quantification sequence. The acquisition parameters were as follows. For axial T2WI: TR/TE of 4000/117 ms; field of view 220 × 220 mm; slice thickness/slice intervals 6/1.8 mm; acquisition time 96 s; and flip angle 90°. For PC-MRI: TR/TE of 21/7 ms; field of view 160 × 160 mm; slice thickness/slice intervals 6/1.2 mm; velocity encoding 15 cm/s; acquisition time ~ 183 s; and flip angle 10°.

2.3 Image analysis

Image processing of the MRI data was performed independently by two radiologists who had 8 and 10 years of experience in brain MRI interpretation, respectively. The plane

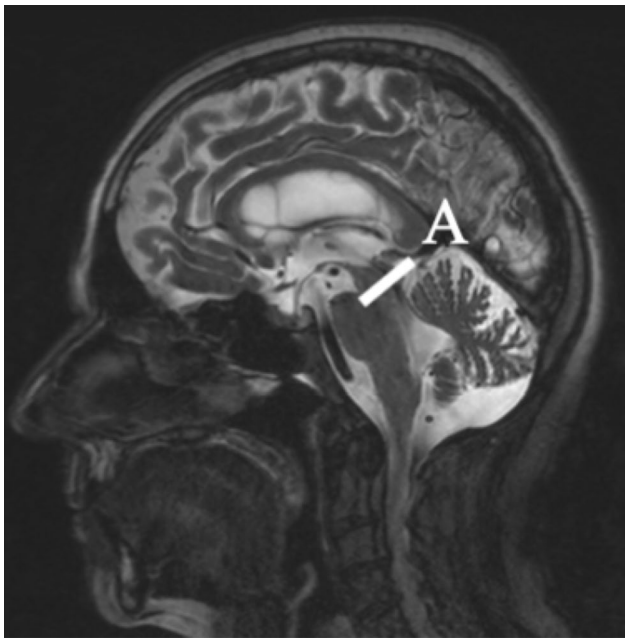

Fig. 1 Midsagittal T2 MRI depicting cerebral aqueduct. Image shows the position of the oblique slices for the cerebral aqueduct (A)

of selection was chosen to pass through the mid-portion of the aqueduct perpendicular to the direction of CSF flow to measure the aqueduct diameter (Fig. 1). Regions of interest in the aqueduct were defined using axial phase images, and the subsequent quantitative analysis of CSF flow was performed using the Flow Quantification analysis software (Siemens, Erlangen, Germany) that is available with the magnetic resonance scanner.

2.4 Data Pre-processing

First, for any series data (i.e., aqueduct diameter and average velocity or pressure) $x = x_1, x_2, x_3, \ldots x_n$, the mean and variance were computed as follows:

$$\bar{x}=\frac{1}{n}\sum_{i=1}^{n} x_i,$$

$$\delta^2 = \frac{1}{n}\sum_{i=1}^{n}(x_i-\bar{x})^2.$$

where n is the number of the patient, x_i is the aqueduct diameter, average velocity or pressure of the i-th patient.

If the distance between a time point x_i and its mean $\bar{x}$ satisfies a threshold value $D = |x - x_i| < 3\delta$, then x_i was retained; otherwise, $x_i = \bar{x}$.

Second, the data were smoothed using a Gaussian filtering with a window width of 18 (implemented using MATLAB 2018a, The MathWorks, Inc., Natick, MA, USA).

2.5 Nonlinear least squares

The relationship between the dependent variable y and the independent variables $x_1, x_2, \ldots, x_p$ was calculated as follows.

$y = f(x_1, x_2, \ldots, x_p; b_1, b_2, \ldots, b_m)$, where f denoted a nonlinear function of the undetermined parameters $b_1, b_2, \ldots, b_m$. In this paper, y is pressure and $x_1, x_2, \ldots, x_p$ are aqueduct diameter and average velocity.

The Levenberg–Marquardt method was then incorporated to determine the values of parameters in a nonlinear least squares model based on N sets of observations for variables $x_1, x_2, \ldots, x_p$ and y.

In particular, we performed three calculation steps described as follows:

1. Calculate the residual sum of squares Q:
   First, set the observed data matrix X as:

$$X = \begin{bmatrix} x_{11} & x_{12} & \cdots & x_{1p} & y_1 \\ x_{21} & x_{22} & \cdots & x_{1p} & y_2 \\ \cdots & \cdots & \cdots & \cdots & \cdots \\ x_{n1} & x_{n2} & \cdots & x_{np} & y_n \end{bmatrix} \tag{1}$$

   The initial values of m parameters were defined as $b_i^0 (i = 1, 2, \ldots, m)$, and these values were then used to calculate the residual sum of squares (Q) of N sets of data that is

$$Q = \sum_{i=1}^{N}\left[y_i - \hat{y}_i\right]^2 = \sum_{i=1}^{N}\left[y_i - f\left(x_{i1}, x_{i2}, \ldots, x_{ip}; b_1^0, b_2^0, \ldots, b_m^0\right)\right]^2 \tag{2}$$

   where $\hat{y}_i = f\left(x_1, x_{i2}, \ldots, x_{ip}; b_1^0, b_2^0, \ldots, b_m^0\right)$.
2. Calculate the coefficients a_{ij} and constant terms a_{iy} of the system:
   Second, let $b_i - b_i^0 = \Delta_i (i = 1, 2, \ldots, m)$. According to the principle of least squares, $\Delta_i (i = 1, 2, \ldots, m)$ satisfied the following linear equations

$$\begin{cases} (a_{11}+d)\Delta_1 + a_{12}\Delta_2 + \cdots + a_{1m}\Delta_m = a_{1y} \\ a_{21}\Delta_1 + (a_{22}+d)\Delta_2 + \cdots + a_{2m}\Delta_m = a_{2y} \\ \cdots\ \cdots\ \cdots \\ a_{m1}\Delta_1 + a_{m2}\Delta_2 + \cdots + (a_{mm}+d)\Delta_m = a_{my} \end{cases} \tag{3}$$

   where $a_{ij} = \sum_{k=1}^{N} \frac{\partial f}{\partial b_i}\left(x_{k1}, x_{k2}, \ldots, x_{kp}; b_1^0, \ldots, b_m^0\right) \cdot \frac{\partial f}{\partial b_j}\left(x_{k1}, x_{k2}, \ldots, x_{kp}; b_1^0, \ldots, b_m^0\right), \quad (i, j = 1, 2, \ldots, m)$ $a_{iy} = \sum_{k=1}^{N} \frac{\partial y}{\partial x}\left(x_{k1}, x_{k2}, \ldots, x_{kp}; b_1^0, \ldots, b_m^0\right) \cdot \left(y_k - \hat{y}_k\right), (i, j = 1, 2, \ldots, m)$,

and d was the damping factor. When $d = 0$, the calculation could be considered as the usual Gauss–Newton iteration.

3. Solve Eq. (3) and perform the iterations: Equations (3) were solved to obtain $\Delta_i (i = 1, 2, \ldots, m)$ and then $b_i = \Delta_i + b_i^0$. When $\max_i \left| b_i - b_i^0 \right| = \min_i \left| \Delta_i \right| < eps$, the iteration was ended, where eps is the condition of stopping iteration. Otherwise, $b_i^0 (i = 1, 2, \ldots, m)$ was regarded as the initial value of the parameters, and steps 1 to 3 were repeated until the required accuracy was reached.

2.6 Accuracy

We used the following formulae to calculate the accuracy: Absolute Error = SUM (|Predicted Value—Actual Value|), Relative Error Rate = Absolute Error / Sum of Actual Values, and then Accuracy = (1—Relative Error Rate) × 100%.

2.7 Statistical analysis

All analyses were performed using EmpowerStats (https://www.empowerstats.com) and the statistical package R (version 3.2.3). Descriptive statistics were expressed as the mean ± standard deviation (SD) and were used to summarise the baseline characteristics. The t-test is used to observe whether there is a difference in the data between the training group and the validation group. Bland–Altman plot is used to check the consistency of the two methods. A two-sided P value < 0.05 was considered to be statistically significant.

3 Results

In this study, a total of 203 consecutive participants were screened, and 138 eligible patients recruited. 5 participants were excluded due to poor MRI image quality, 52 participants were excluded during the lumbar puncture because they were diagnosed with obstructive hydrocephalus, and another 8 patients were excluded because they were unwilling to undergo the lumbar puncture or because their ICP could otherwise not be measured. The remaining 138 participant's data were divided into two groups, i.e., a training group (97 participants) and an independent validation group (41 participants), for the further analysis (Fig. 2). The baseline demographic characteristics of the study population are summarised in Table 1.

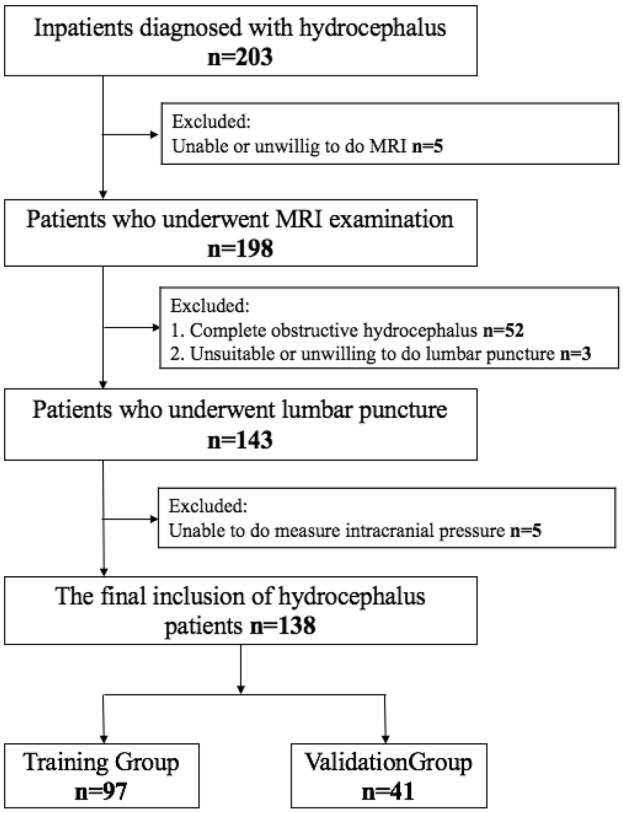

Fig. 2 Flowchart of hydrocephalus participant enrolment

Next, we performed Gaussian filtering on the data to eliminate extreme values, and the processed average velocity, aqueduct diameter and ICP could be obtained. Results are shown in Figs. 3, 4 and 5, in which X-axis represents the number of people in the training group, the blue * in the figure represents the original data, and the red line represents the data after Gaussian filtering.

Using the Levenberg–Marquardt and general global optimisation methods, we modelled the relationships between ICP and both average velocity and aqueduct diameter as follows:

$$Z = P_1 + P_2 * e^{\left(-e^{\left(x - P_3/P_4\right)}\right) - \left(x - P_3/P_4\right) + 1} + P_5 * e^{\left(-e^{\left(y - P_6/P_7\right)}\right) - \left(y - P_6/P_7\right) + 1} + P_8 * e^{\left(-e^{\left(x - P_3/P_4\right)}\right) - \left(x - P_3/P_4\right) + 1} * e^{\left(-e^{\left(y - P_6/P_7\right)}\right) - \left(y - P_6/P_7\right) + 1}$$

Table 1 Baseline characteristics of the studied participants

	Training group (n = 97)	Testing group (n = 41)	P value
Age (year)	57.814 ± 14.518	54.857 ± 20.565	0.736
Heart rate (BPM)	81.827 ± 14.833	81.789 ± 14.135	0.657
SBP (mmHg)	131.778 ± 20.824	128.464 ± 20.729	0.716
DBP (mmHg)	80.526 ± 10.239	79.857 ± 10.027	0.729
BMI	23.798 ± 2.147	24.687 ± 2.543	0.527

P value indicates whether there is a difference between the training group and the independent validation group

BPM beats per minute, *SBP* systolic blood pressure, *DBP* diastolic blood pressure, *BMI* body mass index

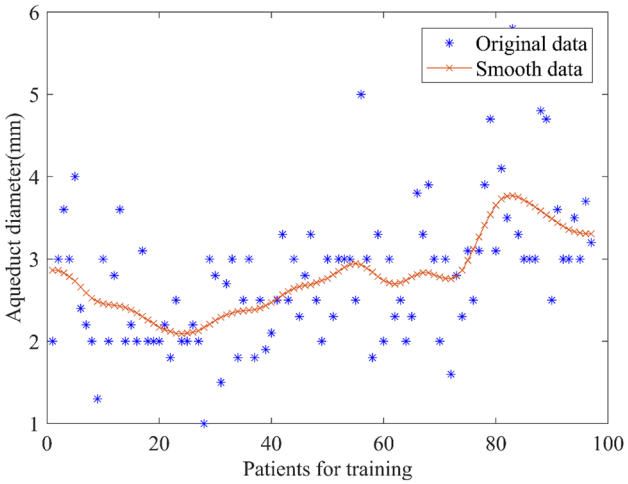

Fig. 3 The original and smoothed data for aqueduct diameter

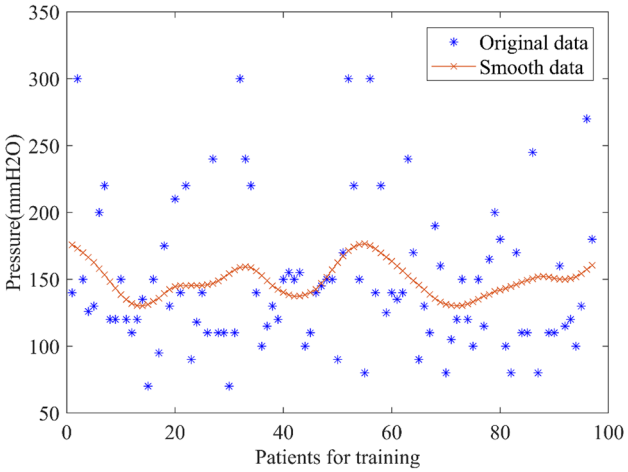

Fig. 5 The original and smoothed data for intracranial pressure

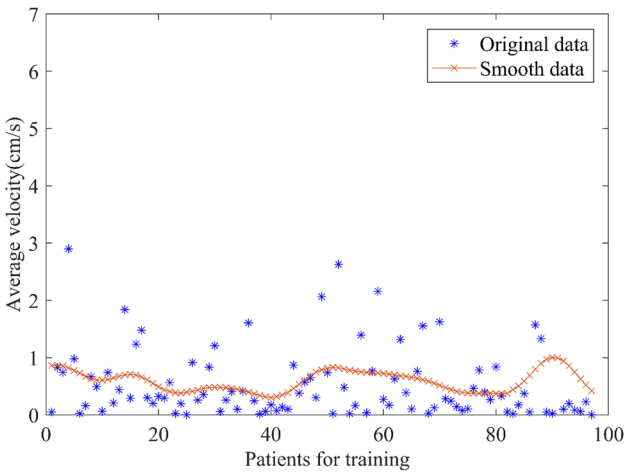

Fig. 4 The original and smoothed data for average velocity

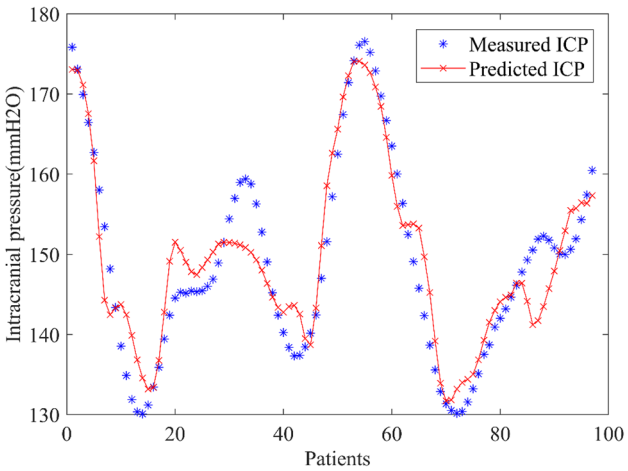

Fig. 6 The relationship between invasively measured (lumbar puncture) intracranial pressure and model-predicted pressure

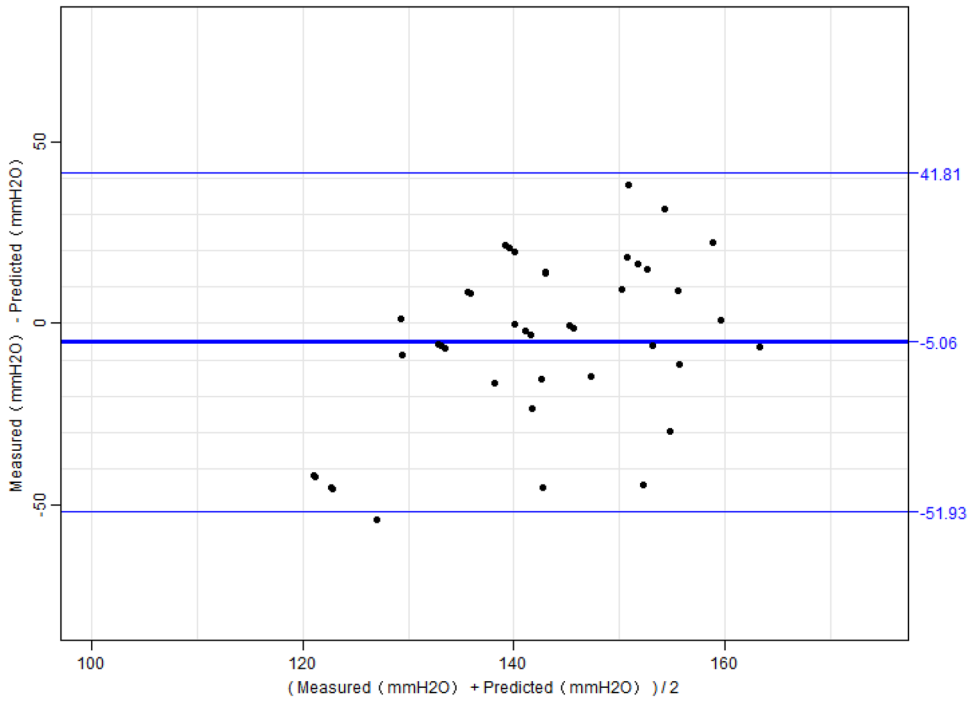

Fig. 7 Bland–Altman plot of model-predicted intracranial pressure and measured (lumbar puncture) pressure

where Z is ICP and X and Y are the average velocity (cm/s) and aqueduct diameter (mm), respectively. The parameters (P) were obtained as $P_1 = 128.32$, $P_2 = 23.21$, $P_3 = 0.49$, $P_4 = -0.15$, $P_5 = 46.88$, $P_6 = 2.96$, $P_7 = 0.32$, and $P_8 = -71.70$.

The fitted results for the measured pressure and the model-predicted pressure are shown in Fig. 6. We obtained a root-mean-square error (RMSE) of 5.42, a sum-of-squared error (SSE) of 2853.09, and a correlation coefficient (R) of 0.899. These results have demonstrated that the relevance of the model fit was very high.

We then tested the model in 41 independent validation participants by inputting the average velocity and aqueduct diameter of each patient into the model to predict their ICP. An analysis of accuracy showed that compared to ICP values obtained using lumbar puncture, the ICP predicted by our model resulted in an accuracy of 86.1% in the independent validation cohort. And draw the Bland–Altman plot to show the consistency test of the model-predicted and lumbar puncture to obtain the intracranial pressure (Fig. 7). The mean of the difference is -5.06 mmH_2O, 95% limits of agreement (-51.93 mmH_2O, 41.81 mmH_2O), 2.43% (1/41) of the points are outside the 95% LoA.

4 Discussion

In this study, we developed and validated a mathematical model for the noninvasive prediction of ICP using nonlinear relationships between ICP and two CSF parameters derived from PC-MRI. The development of this model was based on the Levenberg–Marquardt and general global optimisation methods, which are the most widely used and tested methods for modelling curve-type relationships. We further validated the performance of this model in the noninvasive diagnosis of communicating hydrocephalus based on ICP. We have found that the ICP values predicted by our model have shown excellent performance for estimating ICP in both the training and independent validation cohorts, in which it achieved an accuracy of 0.899 and 0.861. And the Bland–Altman chart shows that 97.5% of the results of the two measurement methods are within the 95% LoA, and the normal value of clinical intracranial pressure fluctuates in the range of 80–180 mmH_2O, respectively, and showed significant agreement with measures obtained using an invasive ICP test (lumbar puncture). Hence, the model developed in this study is accurate and could help clinicians to predict ICP noninvasively.

In previous studies [17, 18], noninvasive MRI based models were designed to predict ICP based on the ratio of intracranial volume changes to ICP gradients. In those models, arterial blood flow velocity, venous blood flow velocity, and CSF velocity were measured to obtain cranial volume. The value of the ICP gradient was then obtained using a complex formula, and the elastic index was then calculated to obtain ICP. While this method was based on rigorous physiological mechanisms, it may take considerable time in specific operations. There is also a distinct difference between the flow velocity and the venous blood flow velocity. If the selected speed encoding value was too high or too low, it

may cause a convolution effect in the phase image, which is substantially different from the real situation. In order to avoid this situation to occur, different speed encoding scans could be chosen within a specific range, and images closer to the real situation are selected for post-processing. However, this procedure takes a long time, making this approach not feasible or efficient for the diagnosis and treatment of emergency patients, such as those with increased ICP. Compared to these previously proposed methods, our developed model only needs to determine the speed coding of the cerebrospinal fluid, which only takes a few minutes.

A previous study [23] also suggested that ICP can be estimated based on the width of the orbital subarachnoid space. This method is similar to our use of aqueduct diameter; however, our model also incorporates a dynamic CSF parameter, i.e., the average velocity. One major difference between our model and the previously proposed models of ICP is that previous models used linear correlation functions, whereas we have utilised a nonlinear function. We advocate this approach because the findings of our previous study have shown that the relationships between ICP and both aqueduct diameter and CSF are nonlinear [20].

The findings from this study have significant clinical value. The current treatment for communicating hydrocephalus is a ventriculoperitoneal shunt [24], which is widely used because it has an adjustable pressure valve that allows the shunt speed to be adjusted in vitro, and this reduces the occurrence of postoperative complications. However, there is little consensus regarding how to set the pressure to achieve the best results. Moreover, this approach, which adjusts the valve speed based on improvement in the patient's clinical symptoms and the clinician's experience, is highly subjective. Furthermore, the invasiveness of the lumbar puncture procedure may also result in postoperative harm [25]. Therefore, our model, which provides a noninvasive strategy for predicting ICP, can be valuable for clinicians because it allows them to adjust the shunt threshold and avoid potential secondary injuries caused by lumbar puncture.

There are limitations to this current retrospective study. First, there were few patients with extremely high ICP values in our study; therefore, when we performed Gaussian filtering, we excluded these extremely high values to ensure the stability of the simulated data. Therefore, our model may not be sensitive in the prediction of extremely high ICP. Second, because we selected only patients with communicating hydrocephalus and excluded those with obstructive hydrocephalus, the proposed model was validated only for communicating hydrocephalus. This limitation could be resolved in future studies that include patients with different types of hydrocephalus. Third, PC-MRI and the lumbar puncture examination were not performed at the same time, and this may have affected our results to some extent, but we do not expect that this factor had a significant impact on our findings. Therefore, experiments in which PC-MRI and lumbar puncture are performed at the same time may represent a useful future research direction to support the noninvasive modelling of ICP.

In conclusion, we developed a mathematical model that predicts ICP in noninvasive PC-MRI derived CSF parameters, such as aqueduct diameter and average velocity. We further validated its accuracy by showing that the results obtained using this model were significantly correlated with those obtained by invasive ICP (lumbar puncture) in communicating hydrocephalus patients. While we do not suggest that PC-MRI should replace invasive ICP monitoring, the proposed model could be potentially helpful for evaluating patients who are poor candidates for invasive procedures.

Author contributions All authors contributed to the study conception and design. All authors commented on previous versions of the manuscript. All authors read and approved the final manuscript. Conceptualization: XH, JH, JX; Methodology: JL, DS, JX, GY; Formal analysis and investigation: XZ; Writing—original draft preparation: JL, DS and XZ; Writing—review and editing: JX, JH and GY; Funding acquisition: JX.

Funding This study was funded in part by the Project of Shenzhen International Cooperation Foundation [Grant Number GJHZ20180926165402083]; in part by the Clinical Research Project of Shenzhen Second People's Hospital [Grant Number 20193357007]; in part by the Clinical Research Project of Shenzhen Health and Family Planning Commission [Grant Number SZLY2018018]; in part by IIAT Hangzhou; in part by the European Research Council Innovative Medicines Initiative on Development of Therapeutics and Diagnostics Combatting Coronavirus Infections Award 'DRAGON: rapiD and secuRe AI imaging based diaGnosis, stratification, fOllow-up, and preparedness for coronavirus paNdemics' [H2020-JTI-IMI2 101005122]; and in part by the AI for Health Imaging Award 'CHAIMELEON: Accelerating the Lab to Market Transition of AI Tools for Cancer Management' [H2020-SC1-FA-DTS-2019-1 952172].

Compliance with ethical standards

Conflict of interest The authors declare that they have no conflict of interest.

Ethics approval All procedures performed in studies involving human participants were in accordance with the ethical standards of the institutional and/or national research committee and with the 1964 Helsinki declaration and its later amendments or comparable ethical standards.

Informed consent Informed consent was obtained from all individual participants included in the study.

References

1. Maira G, Rossi GF, Viganti A. Intracranial pressure and pathogenesis of "normotensive" hydrocephalus. In: Lundberg N, Ponten U,

Brock M, editors. Intracranial pressure II. Berlin: Springer; 1975. p. 128–132.
2. Carney N, Totten AM, O'Reilly C, Ullman JS, Hawryluk GW, Bell MJ, Bratton SL, Chesnut R, Harris OA, Kissoon N, Rubiano AM, Shutter L, Tasker RC, Vavilala MS, Wilberger J, Wright DW, Ghajar J. Guidelines for the management of severe traumatic brain injury. Fourth Edition Neurosurg. 2017;80(1):6–15. https://doi.org/10.1227/NEU.0000000000001432.
3. Hemphill JC, Greenberg SM, Anderson CS, Becker K, Bendok BR, Cushman M, Fung GL, Goldstein JN, Macdonald RL, Mitchell PH, Scott PA, Selim MH, Woo D, American Heart Association Stroke C, Council on C, Stroke N, Council on Clinical C. Guidelines for the management of spontaneous intracerebral hemorrhage: a Guideline for Healthcare Professionals From the American Heart Association/American Stroke Association. Stroke. 2015;46(7):2032–60. https://doi.org/10.1161/STR.0000000000000069.
4. Fried HI, Nathan BR, Rowe AS, Zabramski JM, Andaluz N, Bhimraj A, Guanci MM, Seder DB, Singh JM. The insertion and management of external ventricular drains: an evidence-based consensus statement : a statement for healthcare professionals from the neurocritical care society. Neurocrit Care. 2016;24(1):61–81. https://doi.org/10.1007/s12028-015-0224-8.
5. Long B, Koyfman A. Secondary gains: advances in neurotrauma management. Emerg Med Clin North Am. 2018;36(1):107–33. https://doi.org/10.1016/j.emc.2017.08.007.
6. Ekeh AP, Ilyas S, Saxe JM, Whitmill M, Parikh P, Schweitzer JS, McCarthy MC (2014) Successful placement of intracranial pressure monitors by trauma surgeons. J Trauma Acute Care Surg. 76 (2):286–290; discussion 290–281. doi:https://doi.org/10.1097/TA.0000000000000092
7. Holloway KL, Barnes T, Choi S, Bullock R, Marshall LF, Eisenberg HM, Jane JA, Ward JD, Young HF, Marmarou A. Ventriculostomy infections: the effect of monitoring duration and catheter exchange in 584 patients. J Neurosurg. 1996;85(3):419–24. https://doi.org/10.3171/jns.1996.85.3.0419.
8. Binz DD, Toussaint LG 3rd, Friedman JA. Hemorrhagic complications of ventriculostomy placement: a meta-analysis. Neurocrit Care. 2009;10(2):253–6. https://doi.org/10.1007/s12028-009-9193-0.
9. Kashif FM, Verghese GC, Novak V, Czosnyka M, Heldt T (2012) Model-based noninvasive estimation of intracranial pressure from cerebral blood flow velocity and arterial pressure. Sci Transl Med 4 (129):129ra144. doi:https://doi.org/10.1126/scitranslmed.3003249
10. Michaeli D, Rappaport ZH. Tissue resonance analysis; a novel method for noninvasive monitoring of intracranial pressure. Tech. Note J Neurosurg. 2002;96(6):1132–7. https://doi.org/10.3171/jns.2002.96.6.1132.
11. Ueno T, Ballard RE, Shuer LM, Cantrell JH, Yost WT, Hargens AR. Noninvasive measurement of pulsatile intracranial pressure using ultrasound. Acta Neurochir Suppl. 1998;71:66–9. https://doi.org/10.1007/978-3-7091-6475-4_21.
12. Ragauskas A, Daubaris G, Ragaisis V, Petkus V. Implementation of non-invasive brain physiological monitoring concepts. Med Eng Phys. 2003;25(8):667–78. https://doi.org/10.1016/s1350-4533(03)00082-1.
13. Maissan IM, Dirven PJ, Haitsma IK, Hoeks SE, Gommers D, Stolker RJ. Ultrasonographic measured optic nerve sheath diameter as an accurate and quick monitor for changes in intracranial pressure. J Neurosurg. 2015;123(3):743–7. https://doi.org/10.3171/2014.10.JNS141197.
14. Querfurth HW, Lieberman P, Arms S, Mundell S, Bennett M, van Horne C. Ophthalmodynamometry for ICP prediction and pilot test on Mt. Everest BMC Neurol. 2010;10:106. https://doi.org/10.1186/1471-2377-10-106.
15. Frank AM, Alexiou C, Hulin P, Janssen T, Arnold W, Trappe AE. Non-invasive measurement of intracranial pressure changes by otoacoustic emissions (OAEs)–a report of preliminary data. Zentralbl Neurochir. 2000;61(4):177–80. https://doi.org/10.1055/s-2000-15597.
16. Gwer S, Sheward V, Birch A, Marchbanks R, Idro R, Newton CR, Kirkham FJ, Lin JP, Lim M. The tympanic membrane displacement analyser for monitoring intracranial pressure in children. Childs Nerv Syst. 2013;29(6):927–33. https://doi.org/10.1007/s00381-013-2036-5.
17. Alperin NJ, Lee SH, Loth F, Raksin PB, Lichtor T. MR-Intracranial pressure (ICP): a method to measure intracranial elastance and pressure noninvasively by means of MR imaging: baboon and human study. Radiology. 2000;217(3):877–85. https://doi.org/10.1148/radiology.217.3.r00dc42877.
18. Burman R, Shah AH, Benveniste R, Jimsheleishvili G, Lee SH, Loewenstein D, Alperin N. Comparing invasive with MRI-derived intracranial pressure measurements in healthy elderly and brain trauma cases: A pilot study. J Magn Reson Imaging. 2019;50(3):975–81. https://doi.org/10.1002/jmri.26695.
19. Zhao YL, Zhou JY, Zhu GH. Clinical experience with the noninvasive ICP monitoring system. Acta Neurochir Suppl. 2005;95:351–5. https://doi.org/10.1007/3-211-32318-x_72.
20. Tsivgoulis G, Alexandrov AV, Sloan MA. Advances in transcranial Doppler ultrasonography. Curr Neurol Neurosci Rep. 2009;9(1):46–544. https://doi.org/10.1007/s11910-009-0008-7.
21. Jonas JB, Pfeil K, Chatzikonstantinou A, Rensch F. Ophthalmodynamometric measurement of central retinal vein pressure as surrogate of intracranial pressure in idiopathic intracranial hypertension. Graefes Arch Clin Exp Ophthalmol. 2008;246(7):1059–60. https://doi.org/10.1007/s00417-008-0780-0.
22. Long J, Lin H, Cao G, Wang MZ, Huang XJ, Xia J, Sun Z. Relationship between intracranial pressure and phase-contrast cine MRI-derived measures of cerebrospinal fluid parameters in communicating hydrocephalus. Quant Imaging Med Surg. 2019;9(8):1413–20. https://doi.org/10.21037/qims.2019.08.04.
23. Xie X, Zhang X, Fu J, Wang H, Jonas JB, Peng X, Tian G, Xian J, Ritch R, Li L, Kang Z, Zhang S, Yang D, Wang N, Beijing i COPSG. Noninvasive intracranial pressure estimation by orbital subarachnoid space measurement: the Beijing Intracranial and Intraocular Pressure (iCOP) study. Crit Care. 2013;17(4):R162. https://doi.org/10.1186/cc12841.
24. Pinto FCG, Ureña FDRM. Hydrocephalus basic concepts and initial management. Fundamentals of Neurosurgery. Cham: Springer; 2019. p. 147–160.
25. Eide PK, Sorteberg W (2008) Changes in intracranial pulse pressure amplitudes after shunt implantation and adjustment of shunt valve opening pressure in normal pressure hydrocephalus. Acta Neurochir (Wien) 150 (11):1141–1147; discussion 1147. doi:https://doi.org/10.1007/s00701-008-0138-8

Publisher's Note Springer Nature remains neutral with regard to jurisdictional claims in published maps and institutional affiliations.